Effect of single winding helical electromagnetic stirring on microstructure and mechanical properties of semi-solid Al-Mg_2Si in-situ composites

***Dong Pan[1], Qing-tao Guo[1], Yi-tong Wang[1], Bing-jun Lu[3], Xue-feng Tang[2], Hua-song Liu[1], Pei Xu[1], Xiao-lei Zhu[4], Chong-yi Wei[2], and Yu Zhang[1]**

1. Ansteel Beijing Research Institute Co., Ltd., Beijing 102211, China
2. Technology Center of Angang Steel Co., Ltd., Anshan 114009, Liaoning, China
3. Benxi Steel Plate R & D Institute, Benxi 117000, Liaoning, China
4. Technology Center of Lingyuan Iron and Steel Co., Ltd., Lingyuan 122500, Liaoning, China

Copyright © 2025 Foundry Journal Agency

Abstract: The Al-Mg_2Si in-situ composite is a lightweight material with great potential for application in fields such as automotive lightweighting, aerospace, and electronic components. In this research, the modification, semi-solid technology coupled with different types of electromagnetic stirring was applied to regulate the undesirable solidified dendritic microstructure and facilitate the composites' mechanical properties. The spheroidization and refinement of Mg_2Si and α-Al matrix in SM (semi-solid)+RES (rotate electromagnetic stirring) sample and SM+SHES (single winding helical electromagnetic stirring) sample are realized under the effect of fused dendrite arm, the decreased critical nucleate radius, and the increased nucleation rate and extra supercooling degree induced by electromagnetic stirring. The Mg_2Si phase in the SM+RES sample and SM+SHES sample is refined by 73.4% and 75.7%, respectively compared to the AC (as-cast) sample. Besides, the single winding electromagnetic stirring can lead to more homogeneously distributed physical fields, lower temperature gradient, and more significant mass transfer, mainly responsible for the more homogeneous distributed reinforced finer Mg_2Si particles in the SM+SHES sample. Moreover, both the tensile properties and hardness of modified semi-solid composites are improved through electromagnetic stirring. Compared with RES, the improvement effect of SHES is more excellent. The SM+SHES sample possesses the highest Brinell hardness (124.7 HB), and its quality index of tensile properties is 5.73% and 82.2% higher than that of the SM+RES and AC samples, respectively.

Keywords: electromagnetic stirring; Al-Mg_2Si composites; semi-solid; mechanical properties; modification

CLC numbers: TG146.21 **Document code:** A **Article ID:** 1672-6421(2025)04-449-14

1 Introduction

At present, energy shortages and environmental degradation are becoming increasingly severe. In this context, developing high-performance, lightweight materials is in line with the purpose of energy conservation and emission reduction. Compared with steels, the Al-Mg_2Si composites are widely applied to manufacturing brake discs and engine liners because of the high wear resistance, low density, low thermal expansion, and low cost [1-3]. In this material, the Mg_2Si reinforced particle is an intermetallic compound in-situ formed during solidification [4]. Compared with adscititious particle reinforced (ex-situ) Al-based composites [5, 6], the Al-Mg_2Si composites possess better bonding interface between matrix and particulate, whereas, due to the influence of stress concentration at the sharp edges of the primary Mg_2Si and dendritic matrix in as-cast composites, the mechanical performance is deteriorated [7]. Furthermore, the eutectic Mg_2Si generally fails to prevent crack propagation under mechanical deformation [8]. Therefore, to improve the performance of Al-Mg_2Si composites, the

---

***Dong Pan**

Born in Linyi, Shandong, Ph. D. His research interests primarily focus on thermal simulation of solidification structure of continuous casting billets, electromagnetic stirring of liquid metals, electroinduced toughening of solid metals, and development of special steel products. To date, he has published over 20 papers in SCI, EI, and CA indexed journals, and possesses three invention patents of China.

E-mail: agbjyPD@163.com

Received: 2024-09-10; Revised: 2024-11-01; Accepted: 2024-11-07

homogenization, refinement, densification, and spheroidization of the composites are effective strategies, and dispersion Mg_2Si particles combined with the fine equiaxed α-Al matrix are desirable microstructure.

The properties of materials depend on their microstructure, and the design of the microstructure is closely related to the processing technology. Firstly, the addition of modifiers, such as P, Bi, Sr, Ce, Sb, Mn, and Y [9-11], can break the dendritic morphology of primary Mg_2Si and promote its transformation from different polygonal shapes into spherical particles and dispersion distribution on the matrix. Tebib et al. [12] reported that the Sr+P modifier can facilitate the morphology transformation of Mg_2Si from a coarse dendritic to a fine polygonal shape, and the addition of Sr transformed the morphology of the π-Fe ($Al_8Mg_3FeSi_6$) from a script-like to a fine twin platelet form. Wang et al. [13] found that despite the effect of Sb on nucleation rate, the Sb can replace the position of Si in the lattice and suppress the growth of Mg_2Si along <100> crystal direction, in this way, both the size and the morphology of Mg_2Si are regulated. Heterogeneous nuclei are also an important mechanism for the refinement of Mg_2Si as well as the adsorption poisoning mechanism. As was explored [14], the addition of Sb can also promote the formation of Mg_3Sb_2 which is the heterogeneous nucleation core for Mg_2Si. Among all modifiers, Cu-14wt.% P modifier has good modification effect and low cost [44], so it is selected to modify the Al-Mg_2Si composites in this study. However, achieving only the refinement of reinforced particles is inadequate, and the α-Al matrix should also be refined to further improve the mechanical properties of the composites.

The semi-solid thixoforming technology is an effective method for deriving compact non-dendritic matrix structures [15]. Li et al. [16] found that the dendritic structure of AZ91D magnesium alloy was transformed into a spherical structure after semi-solid isothermal heat treatment, and the average size of the primary phase also decreased significantly. Moreover, combined with electromagnetic stirring, the segregation, central porosity, and other casting defects will be relieved more remarkably by semi-solid technology. In Nourouzi's work [17], the particle size in A356 alloy prepared by a semi-solid rheocasting process combined with electromagnetic stirring was refined, and tensile properties were also improved. So, the application of electromagnetic stirring in the semi-solid casting process is a promising strategy for the quality-upgradation of aluminum alloy ingots.

Compared with conventional rotary electromagnetic stirring (RES), helical electromagnetic stirring (HES) exhibits more tremendous potential in accelerating the mass/heat transfer of molten metal in a three-dimensional direction, the simultaneous solidification, and the alleviation of ingot defects [18]. Interestingly, our team creatively proposed the single-winding helical electromagnetic stirring (SHES) technology [19, 20], and helical stirring of the metal melt can be achieved through only one set of coils. The inherent drawbacks of the complex type HES technology (composed of a combination of traveling wave stirrer and rotary stirrer), such as large volume and mutual shielding of internal and external magnetic fields, can also be avoided. However, the adoption of SHES in semi-solid technology is rarely reported. Thus, the effect of SHES on microstructure and properties of Al-Mg_2Si composites is worth studying.

Therefore, in this contribution, the SHES was used in the synthesis of modifier-treated Al-Mg_2Si composites through semi-solid thixoforming to design a microstructure consisting of globular matrix and reinforcing particles. Based on this, the RES technique was applied to compare the effects of different stirring methods on the modification of Al-Mg_2Si composites. What's more, the finite element simulation was performed to show the difference of physical fields distribution between RES and HES. This research aims to provide valuable insights for producing composites with superior mechanical properties.

2 Experimental procedure

2.1 Preparation process of Al-Mg_2Si composites through semi-solid technology

The commercial pure magnesium, pure aluminium, Al-29wt.% Si master alloy, Cu-14wt.% P modifier were used as initial materials, and the purity of pure aluminium and magnesium was higher than 98%. The detailed weight of each initial material is listed in Table 1. It can be seen that the weight percentage of primary Mg_2Si was determined to be 15%, and P in Cu-14wt.% P accounts for 0.4wt.% of the total composite material. Figure 1 shows the preparation process of semi-solid Al-Mg_2Si composites. The Al-29wt.% Si alloy and pure aluminium were firstly put into a graphite crucible (*Φ*50 mm×100 mm) and melted at 760 °C. After 15 min, the pure magnesium was added, followed by the addition of an appropriate amount of refining agent (KBF_4+K_2TiF_6+K_2ZrF_6), and held for 10 min at 700 °C. Then, removed the slag on the melt surface and raised the temperature to 850 °C. Finally, the Cu-14wt.% P modifier was mixed into the molten metal and kept it fully dissolved. The molten metal was poured into a tungsten steel mold preheated at 200 °C, and then, a gravity casting composites sample was synthesized. It was machined into a slice (100 mm×80 mm×12 mm). The as-cast (AC) sample was used to determine the temperature of the solid-liquid phase region and to observe the microstructure of the composites before it was electromagnetically stirred.

Subsequently, the as-cast composites were remelted at 700 °C and then cooled to semi-solid temperature and ensure that the solid fraction was 25%, the exact value of temperature was about 603 °C (the reason will be given in the later section). The RES and SHES were applied to the semi-solid slurry

Table 1: Detailed weight of each initial material

Initial materials	Al-29Si	Al	Mg	Cu-14P
Weight (g)	200	545	80	25

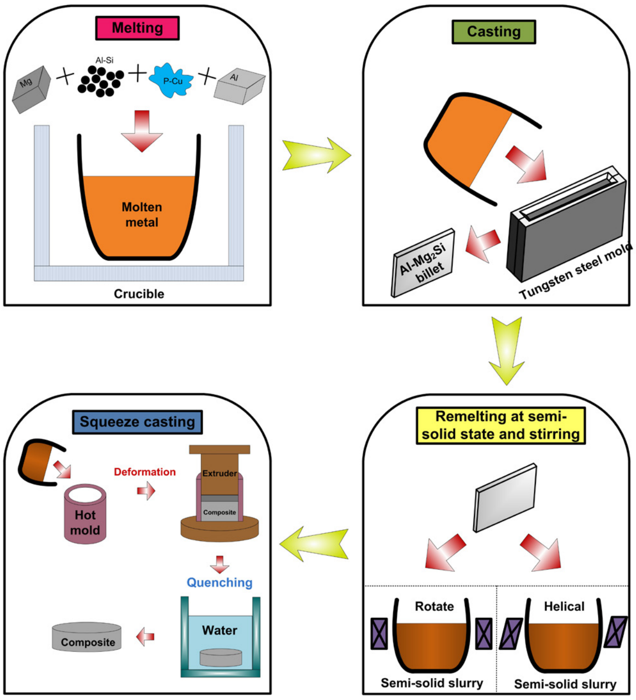

Fig. 1: Preparation process of Al-Mg$_2$Si semi-solid composites

during the isothermal procedure. The stirring frequency and time were 30 Hz and 15 min, respectively. The appearance of SHES apparatus is shown in Fig. 2(a). The corresponding structure of the magnetic yoke is given in Fig. 2(b). As for the RES apparatus, its appearance is the same as that in Fig. 2(a). But, it does not contain the internal magnetic yoke in Fig. 2(b).

After electromagnetic stirring treatment, the semi-solid slurry was poured into a cylindrical die preheated at 300 °C, and was squeeze cast under a hydraulic press. The load was approximately 200 MPa, and the whole process lasted 0.5 min. Then, the squeeze cast composites were quenched to room temperature by water. Meanwhile, other samples, which were electromagnetic stirred, but without squeeze casting, were directly cooled to room temperature in this way, the so called undeformed samples were prepared to compare the effect of electromagnetic stirring method on element segregation of Al-Mg$_2$Si composites.

2.2 Detection and characterization methods

The DSC test was conducted using an SDT Q600 synchronous thermal analyzer to determine the temperature of phase transformation. All the samples were polished with #200–#2000 sandpapers and were etched with 0.05% hydrofluoric acid (HF) solution for microstructure observation. The extraction of primary Mg$_2$Si was conducted by sodium hydroxide (NaOH). The microstructure detection was carried out by an Axio Imager 2 Pol typed optical microscope (OM) and an Axia-Chemi typed scanning electron microscope (SEM). The Image Pro Plus® software was used for statistical analysis of the average size of primary Mg$_2$Si. The D/max 2500 PC typed X-ray diffractometer was used for the phase analysis of the composites in a 2θ range of 15°–90° (Cu Kα) at the scanning rate of 1°·min^{-1}. The tensile test was conducted through the MTS-810 typed tensile machine, and the tensile rate was about 0.5 mm·min^{-1}. The samples for the tensile test possessed a "dog-bone" shape, and the size was: 80 mm (length)×10 mm (width)×6 mm (gauge width)×32 mm (gauge length)×5 mm (transition circle radius). The hardness of the composites was tested by an HB 3000 C typed hardness tester. The macrostructure observation of undeformed (without squeeze casting) electromagnetic stirred composites and the detection of element segregation were conducted to measure the stirring effect. The undeformed electromagnetic stirred composites for macrostructure observation were etched by Keller's reagent (2.5% nitric acid+1% hydrochloric acid+1% hydrofluoric acid+95.5% water) for about 15 s at room temperature. For solute element segregation, an ICP test of the drilled chips at the upper, middle, and lower points on the center line of the longitudinal section of the composites was conducted using a Plasma 3000 tester to measure the distribution of Si and Mg content.

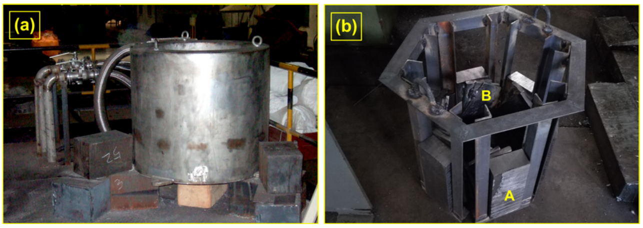

Fig. 2: Single winding helical electromagnetic stirring apparatus (a) and internal magnetic yoke structure (b); A-Yoke back, B-Inclined yoke to generate helical electromagnetic force

2.3 Finite element numerical simulation model

The numerical simulation was performed using ANSYS® software (Technology Center of Angang Steel Co., Ltd., the license number is No. 1071425) to analyze the influence of different electromagnetic stirring methods on the physical field distribution in Al-Mg$_2$Si composites. The numerical simulation model is shown in Figs. 3(a) and (b). Generally, the direction of electromagnetic stirring force is perpendicular to the coil planes in RES, as seen in Fig. 3(d). By tilting the yoke at a certain angle, the electromagnetic force (F) can be divided into horizontal circumferential force (F_R) and force along the drawing direction (F_T). In this way, the helical electromagnetic force was generated in SHES [Fig. 3(c)]. The inclination angle of the magnetic yoke was 43° in this work. The flow, mass transfer, and heat transfer equations were confirmed as follows. At first, the electromagnetic force (F) is governed by Maxwell equation [21]:

$$F=\frac{1}{\mu}(\nabla\cdot B)B-\nabla\left(\frac{B^2}{2\mu}\right) \tag{1}$$

where B and μ are magnetic flux intensity and magnetoconductivity, respectively. The flow equation is based on the Navier-Stokes equation:

$$\frac{\partial(\rho u)}{\partial t}+(\rho u\cdot\nabla)u=-\nabla p+\eta_{\mathrm{eff}}\nabla^2 u+\rho g+F \tag{2}$$

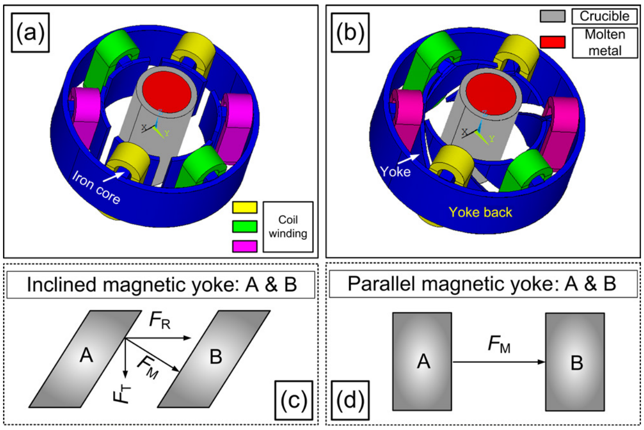

Fig. 3: Model of electromagnetic stirring: (a) RES stirrer; (b) SHES stirrer; The formation mechanism of electromagnetic force in SHES (c) and RES (d); F_M means electromagnetic stirring force; F_R was circumferential component force of F_M, and F_T was component force of F_M along horizontal direction

In Eq. (2), u means flow velocity, ρ is density, g refers to gravitational acceleration, and the η_{eff} is effective viscosity. The mass conservation equation can be expressed as [22]:

$$\frac{\partial \rho}{\partial t} + \nabla \cdot (\rho u) = 0 \tag{3}$$

where t is the time. Finally, for the heat transfer equation, the relationship between the heat generated by the Joule heating effect (Q), the thermal conductivity (K_h), the specific heat (C_p), and the temperature (T) is [22]:

$$Q = \rho C_p \frac{\partial T}{\partial t} - \nabla \cdot K_h \nabla T \tag{4}$$

3 Results and discussion

3.1 Microstructure of Al-Mg_2Si composites

The characterization results of the AC sample are depicted in Fig. 4. According to results in Fig. 4(a), the extrapolated onset temperature of the DSC curve is 545 °C, the endothermic peak temperature is 583 °C, and the extrapolated end temperature is 613 °C. Therein, the solidus and liquidus temperature (T_L) are 583 °C and 613 °C, respectively. The solid fraction (f) of semi-solid slurry is related to the melting point of pure aluminium (T_M), the semi-solid isothermal temperature (T), and the equilibrium partition coefficient (k) [23]:

$$f = 1 - \left[\frac{(T_M - T)}{(T_M - T_L)}\right]^{-\frac{1}{1-k}} \tag{5}$$

In order to maintain the solid fraction of semi-solid slurry at 25%, the isothermal temperature should be 603 °C (Section 2.1).

Based on the results of Figs. 4(b), (c), and (d), it is indicated that the AC sample is composed of primary Mg_2Si [marked as B in Fig. 4(c)], eutectic Mg_2Si [marked as C in Fig. 4(c)], α-Al matrix [marked as A in Fig. 4(c)] and eutectic Si [marked as D in Fig. 4(c)]. The α-Al in AC sample showing a typical dendritic structure, and fishbone like eutectic Si and octahedral primary Mg_2Si are also observed. Because of the addition of Cu-14wt.% P, the characteristic peaks of Al_2Cu are detected in Fig. 4(b).

The microstructure of rotate electromagnetic stirred semi-solid (SM+RES) composites and helical electromagnetic stirred semi-solid (SM+SHES) composites is demonstrated in Fig. 5. Compared with the AC sample, the microstructure of

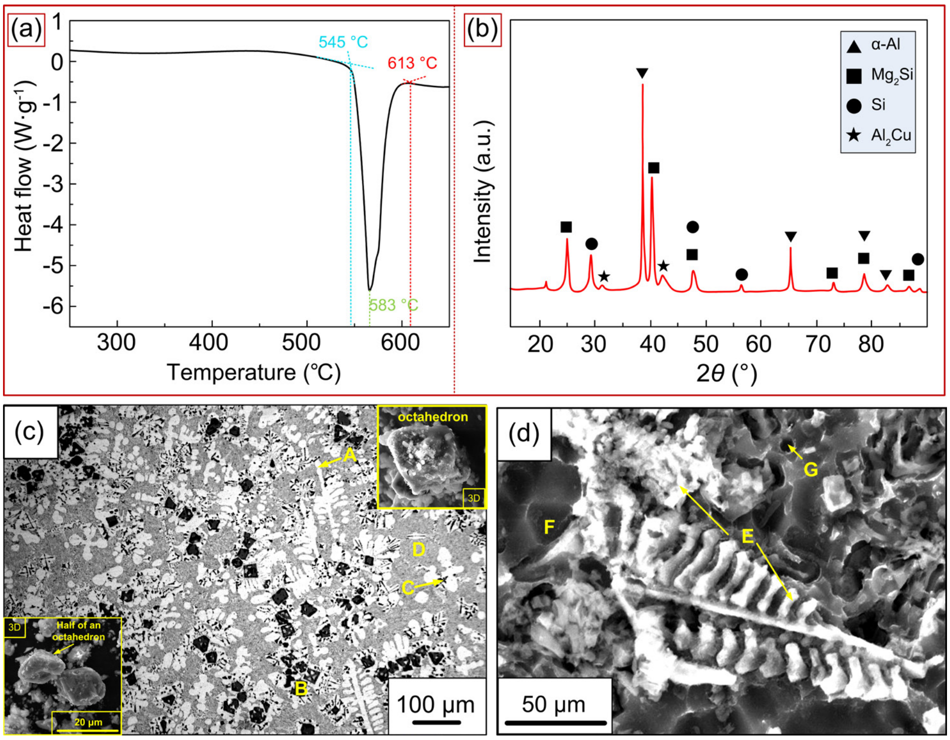

Fig. 4: DSC curve (a), XRD patterns (b), OM image (c), and SEM image (d) of as-cast Al-Mg_2Si composites. E-eutectic Si; F-primary Mg_2Si; G-eutectic Mg_2Si

electromagnetic stirred semi-solid composites is remarkably refined, and the corresponding shape of Mg_2Si is near spherical or irregular granular. Moreover, the α-Al phase is also significantly spheroidized. The transformation of morphology of Mg_2Si can be attributed to the adsorption of P element on the {100} surface, which induces the value of growth velocity between <100> and <111> crystal direction close to $3^{0.5}/3$ [24]. More important, in the semi-solid forming process, the crushing effect of mechanical deformation can lead to the fracture of dendrites, and these broken dendrites can be regarded as nucleation cores to promote the improvement of nucleation rate. Furthermore, the suppression of growth by rapid water cooling is the main reasons for the refinement of Mg_2Si and α-Al.

The size range of Mg_2Si in different samples is presented in Fig. 6, and the morphology factor (K) of Mg_2Si is listed in Table 2. For the mathematical expression of K, it is seen as below [25]:

$$K = \frac{\sum 4\pi A / P^2}{n} \tag{6}$$

where n is the number of Mg_2Si; A and P are the area and perimeter of Mg_2Si, respectively. The closer the value of K is to 1, the closer the morphology of Mg_2Si is to perfect spherical. The results in Fig. 6 imply that the average size order of Mg_2Si is AC>SM+RES>SM+SHES. That's to say, compared with the SM+RES sample, the Mg_2Si in the SM+SHES sample is finer, and the size is decreased by about 8.45%. Besides, the morphology of Mg_2Si in electromagnetic stirred samples is closer to spherical than the AC sample. Compared with the

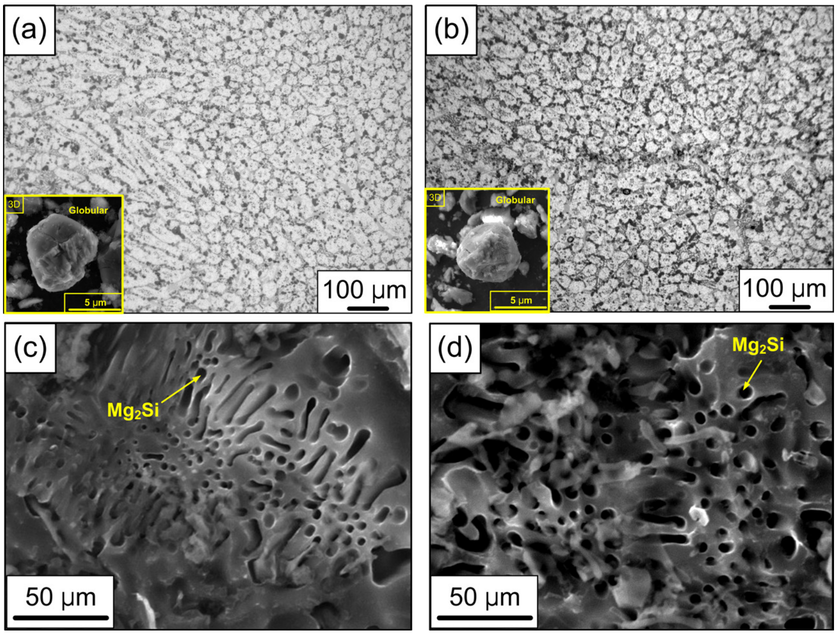

Fig. 5: OM (a, b) and SEM (c, d) images of rotate electromagnetic stirred (a and c) and helical electromagnetic stirred (b and d) samples

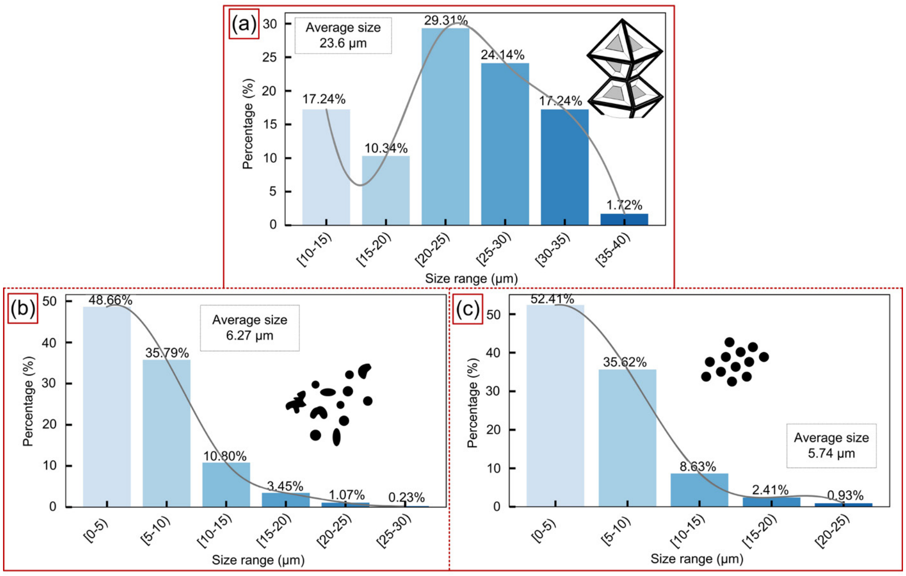

Fig. 6: Statistical data of size distribution of Mg_2Si in different samples: (a) AC sample; (b) SM+RES sample; (c) SM+SHES sample

Table 2: Value of morphology factor of different samples

Sample	AC	SM+RES	SM+SHES
Value of *K*	0.62	0.93	1.04

SM+RES sample, the Mg_2Si in the SM+SHES sample is more rounded. Moreover, the size distribution of Mg_2Si and α-Al in the SM+SHES sample is more homogeneous than that in the SM+RES sample, and this difference will be analyzed later.

3.2 Mechanical properties of Al-Mg_2Si composites

The change in microstructure will necessarily cause a difference in mechanical properties. In this section, the hardness and tensile strength are executed to evaluate the mechanical properties. The calculation expression of Brinell hardness (HB) is:

$$\mathrm{HB} = \frac{\sum_{i=1}^{n} \frac{0.204F}{\left[\pi D_\mathrm{b}\left(D_\mathrm{b} - \sqrt{(D_\mathrm{b}^2 - d_i^2)}\right)\right]}}{n} \tag{7}$$

where n is the number of the hardness test points, the F refers to the load, the D_b is the diameter of indenter, and the d_i means the diameter of the ith indentation. The Q index is used to reflect the quality of tensile properties, and it is explained as a semilogarithmic plot of the ultimate tensile strength (UTS) versus the fracture elongation (EL%) [26]: Q=UTS (MPa) +150×log(EL%). The results of mechanical properties are shown in Fig. 7, and the data are listed in Table 3. It's indicated that the value of mechanical properties of AC sample is relatively lower. Compared with AC sample, the hardness, tensile strength, and ductility of electromagnetic stirred samples are enhanced simultaneously. Compared to SM+RES sample, the SM+SHES sample exhibits better mechanical properties. The highest value of tensile properties Q index (418.6) is acquired by single-winding helical electromagnetic stirring, resulting in the highest Brinell hardness (124.7 HB). The tensile properties of SM+SHES sample are about 5.73% and 82.2% higher than the SM+RES sample and AC sample, respectively.

The tensile strength (σ) is remarkably influenced by the grain size of the matrix (D_α) and the size of reinforced particles (d_r), which can be explained by the equation below [27-29]:

$$\sigma \propto \eta_\mathrm{k} D_\alpha^{-1/2} \approx d_\mathrm{r}^{-1/2} \left(\frac{V_\mathrm{m}}{V_\mathrm{r}}\right)^{1/6} \tag{8}$$

where the η_k is the morphology factor, and the V_m and V_r are the volume fraction of the matrix and reinforced particles, respectively. Thus, it's obvious that the SM+SHES sample possesses the highest value of tensile properties Q index and hardness. Apart from the value of mechanical properties, the descending order of error limits for hardness values is AC sample>SM+RES sample>SM+SHES sample. It is proved from the other side that the microstructure of the SM+SHES sample is the most uniform, which is consistent with the results of Fig. 5.

The fracture morphology of samples at different states is given in Fig. 8. In the AC sample, some primary Mg_2Si particles are embedded into the matrix, and these Mg_2Si particles possess complete octahedral morphology. Besides, the crack exists on the surface of some primary Mg_2Si particles, and the propagation direction of the crack is parallel to <100> direction. Moreover, the matrix does not exhibit a typical ductile fracture morphology, and no α-Al adheres to the surface of Mg_2Si. In other words, the primary fracture mode of AC samples is tearing at the bonding interface between the primary Mg_2Si and α-Al matrix. For SM+RES sample and SM+SHES sample, the dimples start to emerge explosively. In the SM+RES sample, the dimples are heterogeneously distributed, indicating the uneven distribution of local deformation. As for the SM+SHES sample, the size distribution of dimples is more homogeneous, and the appearance of tearing ridges in Fig. 8(c) implies better plasticity.

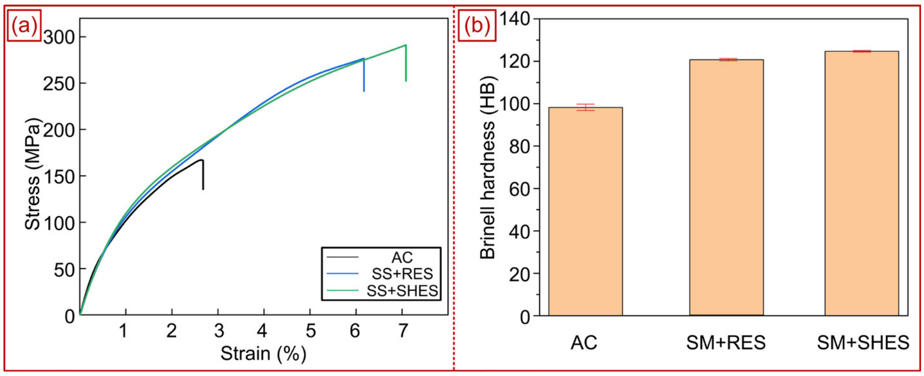

Fig. 7: Mechanical properties of Al-Mg_2Si composites: (a) tensile curves; (b) Brinell hardness

Table 3: Detailed data of mechanical properties of Al-Mg_2Si composites

Sample	UTS (MPa)	Elongation (%)	Q index (MPa)	Hardness (HB)
AC	165	2.7	229.7	98.2±1.6
SM+RES	276	6.3	395.9	120.4±0.6
SM+SHES	290	7.2	418.6	124.7±0.4

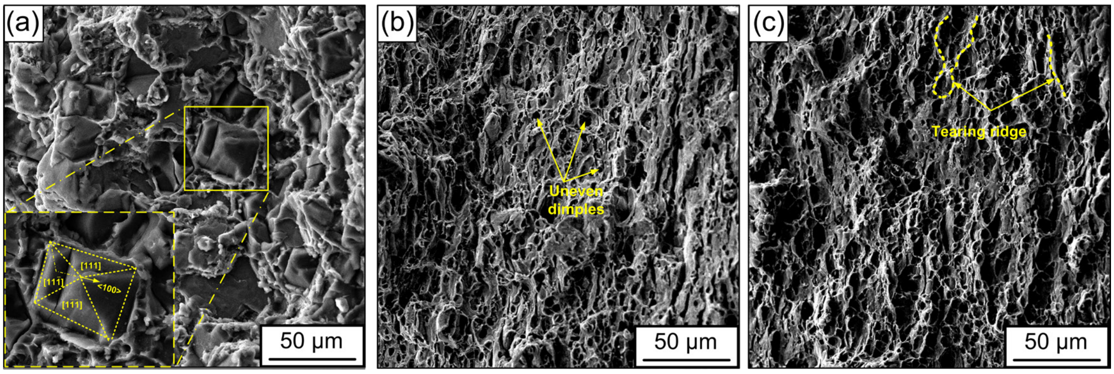

Fig. 8: Fracture morphology of AC sample (a), SM+RES sample (b), and SM+SHES sample (c)

3.3 Difference in stirring effect between RES and SHES

The results in Fig. 5 and Fig. 6 have verify that the Mg_2Si and α-Al in the SM+SHES sample show better roundness, finer size, and more dispersed distribution than those in the SM+RES sample. This must be related to the differences in the distribution of the electromagnetic field, flow velocity field, and temperature field inside the slurry during semi-solid electromagnetic stirring of these two samples.

The simulation results of the electromagnetic field are depicted in Fig. 9. It's declared that most of the electromagnetic force vectors in the semi-solid slurry are distributed in the circumferential direction during RES. For SHES, except for the circumferential direction, the electromagnetic force tends to be distributed along the axial direction. Meanwhile, the magnetic induction intensity profile in RES is symmetrically distributed. However, it has a significant deflection in SHES. The difference in electromagnetic force distribution between these two kinds of electromagnetic stirring will inevitably lead to the distinction between flow velocity field and temperature field distribution.

The qualitative calculations of flow velocity and temperature distribution are unfolded in Fig. 10. It is explained that compared with the linear flow velocity distribution in RES, the metal liquid under the stirrer forms a stagnant zone. This is caused by the counteraction between the gravity effect and the passive reverse flow of liquid metal in the middle region caused by the accelerated downward flow of liquid metal on the surface. As a result, in SHES, a uniform temperature region with a similar shape is found in the corresponding retention zone of flow velocity. However, in RES, a V-shaped temperature distribution region is observed. The quantitative results of flow velocity and temperature distribution are given in Fig. 11. It is shown that the flow velocity along axial direction in SHES is higher than that in RES. In addition, the temperature gradient from surface to center in SHES is also smaller than that in RES. It is well established that the decrease in temperature gradient is helpful for the enhancement of the equiaxed crystal ratio [20], which will be verified by future experimental results.

The flow velocity along the axial direction is closely related to the mass transfer of semi-solid slurry. As can be

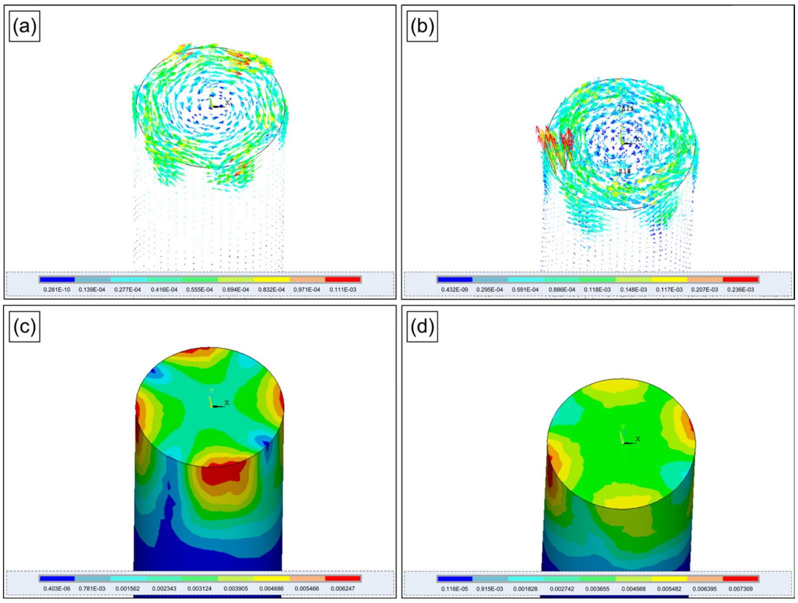

Fig. 9: Electromagnetic force vector distribution in SM+RES sample (a) and SM+SHES sample (b), and contour distribution of magnetic induction intensity in SM+RES sample (c) and SM+SHES sample (d)

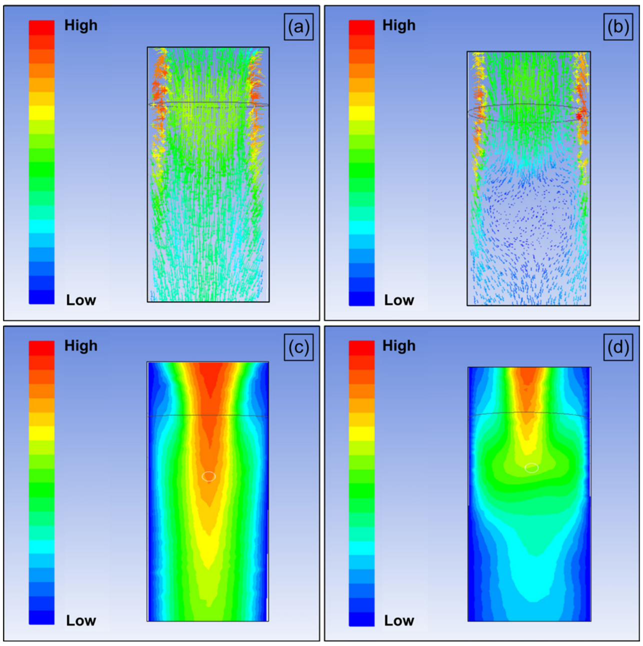

Fig. 10: Flow velocity vector distribution in RES (a) and SHES (b), and temperature contour distribution in RES (c) and SHES (d) at the longitudinal section

seen from the tracer particle motion trajectory in Fig. 12, the tracer particles in RES mainly move along the circumferential direction. However, in SHES, the length of axial movement of tracer particles is longer than that of RES. That is to say, the SHES has a wider mass transfer range than RES.

It is well known that the temperature gradient (G_L) has an essential influence on the morphology of solidified structures [30]:

$$\frac{G_L}{R_v} \geq \frac{m_L C_0(1-k_d)}{k_d D_L} \tag{9}$$

where R_v is the solidification rate. It can be speculated that the decrease in temperature gradient can induce the weakening of constitutional supercooling at the front of the solidified interface, which is beneficial for maintaining the stability of the interface [30]. Thus, the formation of dendritic morphology is inhibited. Also, the preferred growth direction of α-Al is <001> direction, which is parallel to the direction of the temperature gradient. The decreased temperature gradient can also impede the growth of α-Al along the temperature gradient and promote its transformation to equiaxed crystal. Consequently, the morphology of Mg_2Si and α-Al in the SM+SHES sample is more rounded than that in the SM+RES sample.

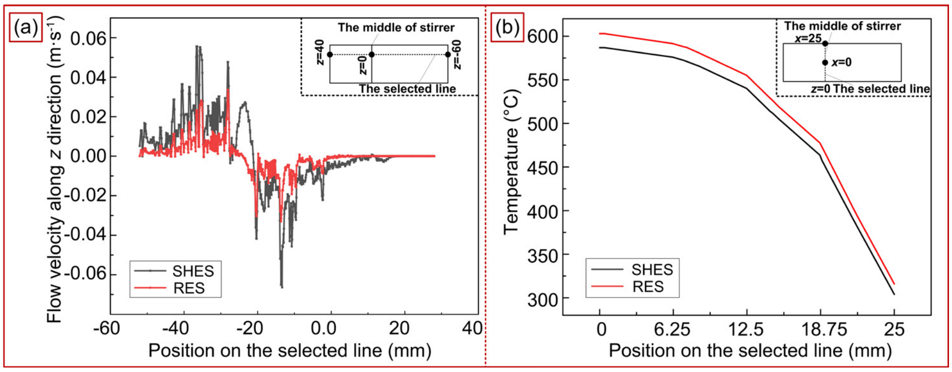

Fig. 11: Quantitative results of flow velocity (a) and temperature (b) along the selected characteristic line; the inserts show the location of the selected characteristic line

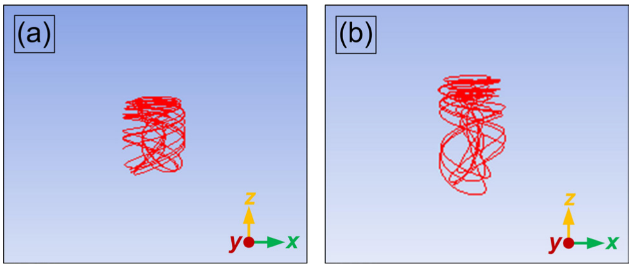

Fig. 12: Tracer particle motion trajectory in RES (a) and SHES (b)

The influence mechanism of flow velocity on the composites is mainly reflected in its impact on dendritic fracture and constitutional supercooling (ΔT_c). The remelting and fusing of the criterion for dendrite (C_R) is [31]:

$$C_R = \frac{u_l}{v_t} > 1 \tag{10}$$

where u_l is the flow velocity along the growth direction of the secondary dendrite arm, and the v_t is the flow velocity perpendicular to the growth direction of the secondary dendrite arm. Therefore, the u_l can be considered as the flow velocity along the axial direction, and the v_t is regarded as circumferential flow velocity. The results in Fig. 11(a) have clarified that the axial flow velocity in the SM+RES sample is smaller than that in the SM+SHES sample. Finally, the dendrites in the SM+SHES sample are easier to remelt than the SM+RES sample.

It should be mentioned that the growth speed (v_g) of the solidified microstructure is mainly governed by the constitutional supercooling (ΔT_c) [32]:

$$v_g = \alpha_2 \Delta T_c^{\,2} + \alpha_3 \Delta T_c^{\,3} \tag{11}$$

where α_2 and α_3 are the growth parameters for solidified microstructure. During the solidification process, the selective crystallization leads to the enrichment of solute elements at the solid-liquid interface, which will result in the formation of constitutional supercooling. Under the effect of the higher axial flow rate in SHES, the diffusion extent of the enriched solute elements in the SM+SHES sample is greater than that in the SM+RES sample. Combined with the results of Fig. 10 and Fig. 12, the solute elements in SM+SHES sample will be more evenly distributed than those in SM+RES sample, which will result in lower constitutional supercooling. Thus, the value of ΔT_c in the SM+SHES sample is lower than the SM+RES sample. Consequently, according to Eq. (11), the growth speed of solidified microstructure in the SM+SHES sample is lower than that in SM+RES sample, and finer Mg_2Si and α-Al are derived. To further study the effect of stirring mode on Al-Mg_2Si composites, the macrostructrue and element distribution of the undeformed samples (composites after electromagnetic stirring without squeeze casting) were characterized, as shown in Fig. 13 and Table 4.

The macrostructures and element distribution of undeformed semi-solid composites are shown in Fig. 13. The sampling section used for macrostructure observation is 1/4 of the whole composites section, and the number in the illustration in Figs. 13(a) and (b) represents the element content detection position at the sampling section. It is seen that compared with the undeformed SM+RES sample, the equiaxed grain rate of the undeformed SM+SHES sample is higher, and the size of the equiaxed grains is also smaller. This further demonstrates the better improvement effect on microstructure in semi-solid Al/Mg_2Si composites caused by SHES induced lower temperature gradient. The values of the Si and Mg content at different positions are given in Table 4. It's seen that the Mg and Si element distribution in the undeformed SM+SHES sample is more homogeneous than the undeformed SM+RES sample, which implies the more homogeneous physical fields and accelerated motion of molten metal induced by SHES. In a word, the experimental results further confirm the above analysis [Eqs. (9–11)] of the influence of differences in the physical field distribution of electromagnetic stirring on the microstructure of composites.

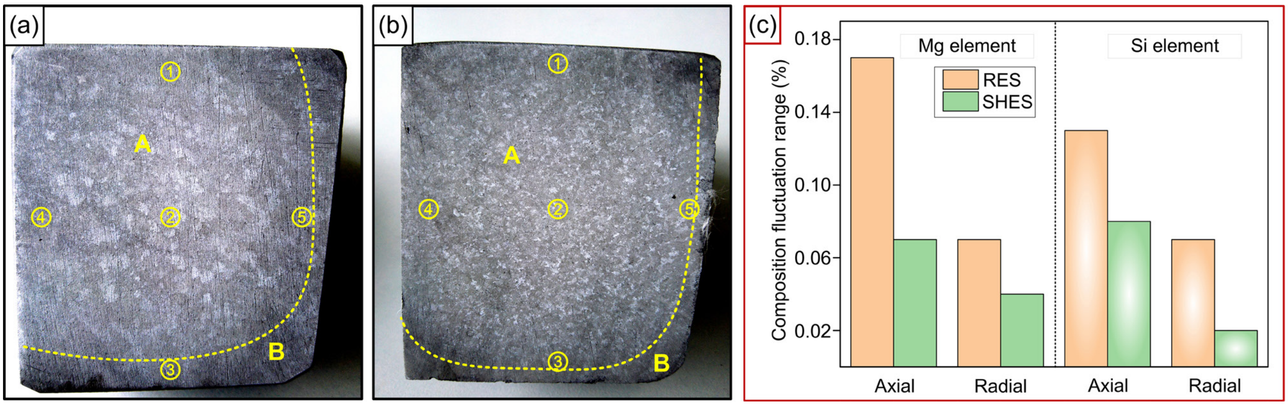

Fig. 13: Macrostructures of undeformed SM+RES sample (a) and undeformed SM+SHES sample (b), and the histogram of Mg and Si content at different positions of the undeformed semi-solid composites (c). A-equiaxed region, B-Dentritic region

Table 4: Element distribution and equiaxed ratio of undeformed electromagnetic stirred Al-Mg_2Si semi-solid composites

Items	Undeformed SM+ SHES sample	Undeformed SM+ RES sample
Content of Mg/Si at Position 1	9.34%/6.74%	9.27%/6.72%
Content of Mg/Si at Position 2	9.41%/6.77%	9.35%/6.76%
Content of Mg/Si at Position 3	9.39%/6.82%	9.44%/6.85%
Content of Mg/Si at Position 4	9.43%/6.79%	9.37%/6.77%
Content of Mg/Si at Position 5	9.45%/6.79%	9.42%/6.83%
Range of Mg/Si content (radial)	0.04%/0.02%	0.07%/0.07%
Range of Mg/Si content (axial)	0.07%/0.08%	0.17%/0.13%
Equiaxed grain rate	95.1%	92.3%

To sum up, the SHES induced constitutional supercooling, lower temperature gradient, and more significant remelting of dendritic arms are responsible for the refinement and spheroidization of the Mg_2Si and α-Al of semi-solid composites. The more comprehensive mass transfer range and the more uniform temperature distribution in SHES are the main reasons for the more homogeneous distribution of Mg_2Si and α-Al in the SM+SHES sample. However, the above discussion is only a qualitative analysis of the influence of differences in physical field distribution on the microstructure of composites, quantitative analysis will be made in next section to deeply research the modification mechanisms of SHES.

3.4 Effecting mechanism of electromagnetic stirring on Al-Mg_2Si composites

As is displayed in Fig. 14, the modification of the microstructure of Al-Mg_2Si composites is the result of the comprehensive effect of multiple factors. The impact of Cu-14% P modifier, deformation after semi-solid treatment, and physical field distribution induced by electromagnetic stirring on the microstructure of the composites has been qualitatively discussed in prior sections. As for the effect of semi-solid

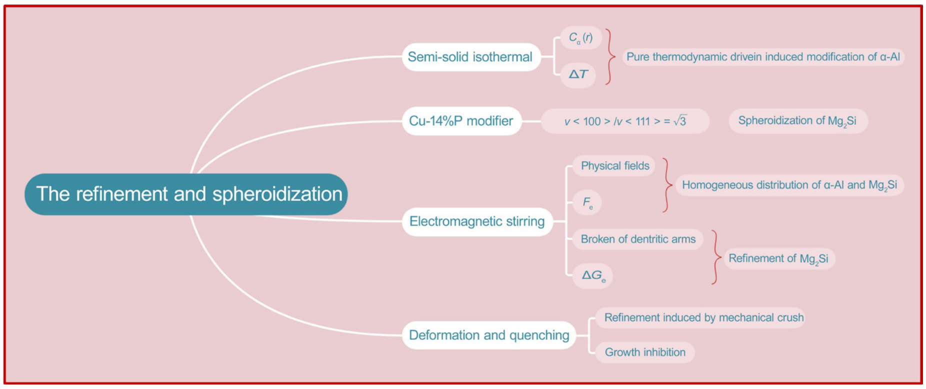

Fig. 14: Logical analysis of microstructure refinement and spheroidization mechanism in Al-Mg_2Si composites

treatment on spheroidization of the microstructure, before the composites are semi-solid treated, there will be a concentration fluctuation of Si atoms at the interface between dendritic α-Al and octahedral Mg_2Si, according to the research from Ma et al [33]. When the composites are heated to a semi-solid temperature, the motion of Si atoms is stimulated. Based on Gibbs-Thomson's theorem [33]:

$$C_\alpha(r)=C_\alpha(\infty)\exp\left(\frac{2\sigma V}{k_0 rT}\right) \tag{12}$$

where r is curvature radius, $C_\alpha(r)$ means solute concentration at the radius of curvature r, $C_\alpha(\infty)$ refers to solute concentration at the planar interface, σ is surface tension, V is the volume of solute atom, T is the temperature, k_0 represents the constant related to morphology. It can be inferred that the accelerated motion of Si atoms will promote the formation of Si diffusion pair at the edge of the octahedral Mg_2Si, which can lead to the dissolution of Mg_2Si at a location where the value of r is relatively lower. Consequently, the Mg_2Si is preliminarily spheroidized.

In addition, the spheroidization of α-Al can be explained by the relationship between the equilibrium melting point (ΔT_e) and curvature radius [33]:

$$\Delta T_e=-\frac{2\sigma T_m V_S r}{\Delta H} \tag{13}$$

where V_S is the molar volume of the solid phase, T_m is the melting point of the interface between solid and liquid, ΔH refers to the molar enthalpy of the solid-liquid transition. It is concluded that the equilibrium melting point of Al dendrites with smaller curvature radii will decrease, resulting in more rounded edges of these α-Al dendrites.

According to Eq. (8), the refinement of Mg_2Si is vital for the enhancement of the mechanical properties of the composites. Besides, the refinement of Mg_2Si is related to the electromagnetic stirring, and the type of electromagnetic stirring is also the main reason for the difference between the SM+RES sample and the SM+SHES sample. Therefore, in the next, the effecting mechanisms of electromagnetic stirring on refinement of Mg_2Si will be deeply explored. The parameters and some important physical quantities proposed from the ANSYS simulation model in Section 3.3 used for following quantitative calculation are listed in Table 5.

Table 5: Parameters of Al-15Mg_2Si composites and physical quantities from ANSYS numerical simulation model

Parameters	Unit	Value
Density of Mg_2Si [34]	$kg\cdot m^{-3}$	1,990
Density of Al-15Mg_2Si melt [34]	$kg\cdot m^{-3}$	2,440
Electrical conductivity of Mg_2Si [34]	$S\cdot m^{-1}$	5.9×10^3
Electrical conductivity of Al-15Mg_2Si melt [34]	$S\cdot m^{-1}$	4.2×10^6
Supercooling of Al-15Mg_2Si melt [34]	K	2
Maximum axial electromagnetic force in RES	$N\cdot m^{-3}$	82
Maximum axial electromagnetic force in SHES	$N\cdot m^{-3}$	47
Maximum radial electromagnetic force in RES	$N\cdot m^{-3}$	1,025
Maximum radial electromagnetic force in SHES	$N\cdot m^{-3}$	1,533
Magnetic field energy induced by RES	$J\cdot m^{-3}$	-4.5×10^{-5}
Magnetic field energy induced by SHES	$J\cdot m^{-3}$	-7.3×10^{-5}

At first, the size of Mg_2Si is determined by the critical nucleation radius (R), which is governed by the change in volume free energy (ΔG_V) [35]:

$$\begin{cases} R=-\dfrac{2\sigma}{\Delta G_V+\Delta G_e} \\ \Delta G_V=-\dfrac{L_m}{T_{melt}}\cdot\Delta T \end{cases} \tag{14}$$

where ΔG_e is the change of volume free energy caused by electromagnetic stirring, ΔT is the supercooling of the melt, T_{melt} is the melting point of Al-15Mg_2Si composites, and L_m is the fusion enthalpy. Both the values of ΔG_e and ΔG_V are negative. Therefore, according to Eq. (14), the ΔG_e will lead to a decrease in critical radius, which is beneficial for the refinement of Mg_2Si. According to Fig. 4(a), the melting point of the composites is 856 K, and the fusion enthalpy is 22.75 $J\cdot g^{-1}$ by calculating the peak area in Fig. 4(a). Thus, the volume free energy is calculated to be –53.15 $J\cdot kg^{-1}$. The values of ΔG_e in SM+RES sample and SM+SHES sample are –0.11 $J\cdot kg^{-1}$ and –0.17 $J\cdot kg^{-1}$, which are converted from the magnetic field energy in Table 5. Based on this, it can be concluded that the critical nucleation radius of Mg_2Si in SM+SHES sample is smaller than that in SM+RES sample. As a result, the Mg_2Si in SM+SHES sample is finer.

The difference in distribution of Mg_2Si in the SM+RES sample and the SM+SHES sample is in relationship with the magnetic induced extrusion force (F). During the electromagnetic stirring process, the Mg_2Si particle will suffer from gravity (F_G), buoyancy (F_b), and magnetic induced extrusion force. The direction of F is opposite to the direction of electromagnetic force (F_e), and the equation of F_e is [36]:

$$F=\frac{\pi d^3}{4}\cdot\frac{\sigma_m-\sigma_p}{2\sigma_m+\sigma_p}F_e \tag{15}$$

where d is the size of the Mg_2Si particle, σ_p and σ_m are the conductivity of the Mg_2Si particle and the melt. For buoyancy and gravity, the expression is [37]:

$$\begin{cases} F_G=\dfrac{\pi d^3}{6}g\rho_p \\ F_b=\dfrac{\pi d^3}{6}g\rho_m \end{cases} \tag{16}$$

where g is gravitational acceleration, ρ_p and ρ_m are the density of the Mg_2Si particle and the melt. According to Table 5 and Fig. 6(a), the buoyancy and gravity are calculated to be 13.41×10^{-11} N and 16.46×10^{-11} N.

The radial magnetic induced extrusion force in the SM+RES sample and SM+SHES sample is 4.22×10^{-13} N and 2.42×10^{-13} N, respectively. The axial magnetic induced extrusion force in the SM+RES sample and SM+SHES sample is 5.27×10^{-12} N and 7.89×10^{-12} N, respectively. The force analysis of Mg_2Si particle during electromagnetic stirring is shown in Fig. 15. It's seen that the resultant force of buoyancy and axial magnetic induced extrusion force is axial and opposite to the gravity direction, and its magnitude also exceeds that of gravity. Hence, the axial magnetic induced extrusion force can avoid the segregation of Mg_2Si particles in the axial direction and promote its axial movement. In addition, the radial magnetic induced extrusion force is easy to cause the accumulation of Mg_2Si particles near the crucible wall. According to calculation results, under the effect of smaller radial magnetic induced extrusion force and higher axial magnetic induced extrusion force in SM+SHES sample, the Mg_2Si particle tends to be more evenly distributed in all directions than SM+RES sample.

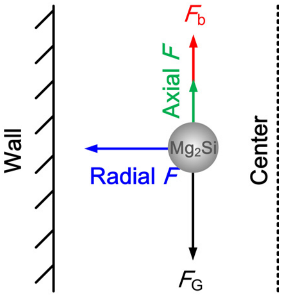

Fig. 15: Force analysis of Mg_2Si particle during electromagnetic stirring

3.5 Summary and outlook

The sketch diagram in Fig. 16 demonstrates the effect of electromagnetic stirring on the microstructure evolution of Al-Mg_2Si composites. It's seen that without the application of electromagnetic stirring, only natural convection will occur in semi-solid slurry, and nearly no disturbance will act on the solidification process of composites. As a result, a dendritic matrix and octahedral Mg_2Si will be obtained. After the electromagnetic stirring is applied, forced convection will occur, and this can lead to the fusing of the secondary dendrite arm. The fused secondary dendrite arm can be regarded as a new nucleation particle to promote the modification of the microstructure. Additionally, combined with the effect of Cu-14% P modifier (without the addition of modifier, the microstructure of composites will have more significant dendritic characteristics [49]) and squeeze casting, refinement and spheroidization of α-Al matrix and Mg_2Si particles are achieved. What's more, compared with RES, helical electromagnetic force induced special electromagnetic fields, unique magnetic induced extrusion force and wider mass transfer region in SHES is favorable for more uniform distribution and further refinement of the microstructure of Al-Mg_2Si composites.

Comparison of tensile properties of Al-Mg_2Si composites between this work and other advanced modification strategies [38-50] is shown in Fig. 17. It's noted that the chemical modifier, heat treatment, and mechanical deformation are beneficial for the improvement of strength, and the semi-solid treatment and electromagnetic stirring are more effective in enhancing ductility. In this research, through the combination of chemical modifier, helical electromagnetic stirring, semi-solid isothermal treatment, and squeeze casting, the strength of Al-Mg_2Si composites has reached an unprecedented level while maintaining relatively higher ductility. However, owing to the lack of deformation and heat treatment on Al-Mg_2Si composites, the ductility still needs further improvement, and more advanced mechanical properties of Al-Mg_2Si composites will be presented in future work.

4 Conclusions

This article systematically investigated the effect of different kinds of electromagnetic stirring on microstructures and mechanical properties of semi-solid Al-Mg_2Si in-situ composites. The following conclusions are drawn as below:

(1) Through the combined treatment of modifier addition, semi-solid isothermal treatment, electromagnetic stirring, and squeeze casting, the spheroidization and refinement of both Mg_2Si and α-Al matrix are successfully achieved. Compared with AC sample, the morphology factor values of SM+RES sample and SM+SHES sample are closer to 1, and the size of Mg_2Si is decreased by 73.4% and 75.7%, respectively.

(2) In contrast to RES, the SHES can induce higher axial electromagnetic force, higher flow velocity, wider mass transfer range, more homogeneous temperature distribution,

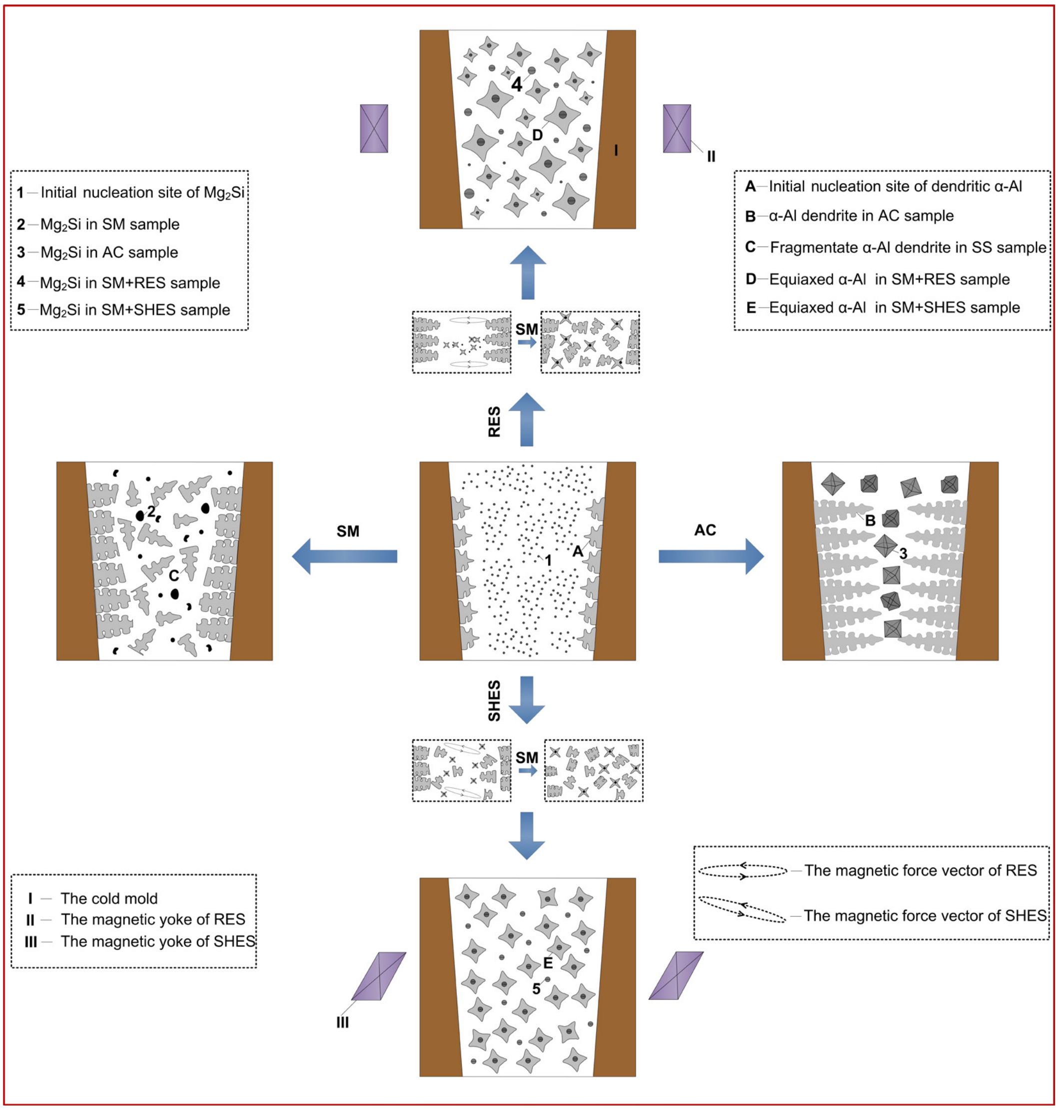

Fig. 16: Sketch diagram showing the effect of different kinds of electromagnetic stirring on microstructure evolution mechanism of Al-Mg_2Si composites

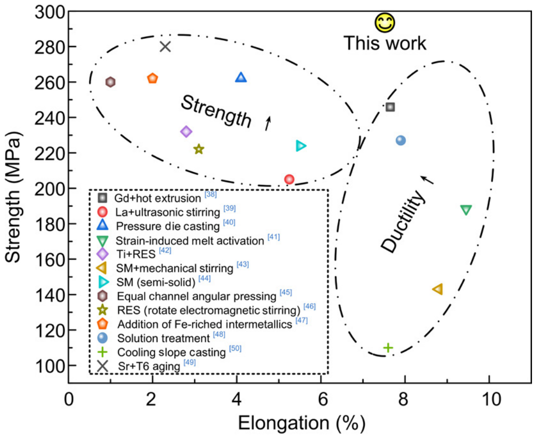

Fig. 17: Statistical comparison of tensile properties of Al-Mg_2Si composites between this work and other advanced modification strategies

and lower temperature gradient. As a result, more uniformly dispersed Mg_2Si and α-Al are derived in the SM+RES sample. The size of Mg_2Si in SM+RES sample is also decreased by 8.45% compared with the SM+RES sample.

(3) The strength, ductility, and hardness of modified semi-solid composites are simultaneously improved by electromagnetic stirring. The SHES has more advantages than RES in improving mechanical properties. The SM+SHES sample exhibits the highest tensile properties which is 5.73% higher than the SM+RES sample, and 82.2% higher than the AC sample.

Acknowledgments

This work was financially supported by the National Key R&D Projects (No. 2021YFB3702000), the Institute Projects of Ansteel Beijing Research Institute (No. 2023BJC-06) and the Regional Company Projects in Ansteel Beijing Research Institute (No. 2022BJB-18BG & No. 2022BJB-13GF). Sincerely thanks Prof. Yu-guang Zhao from Jilin University for theoretical guidance with respect to Al-Mg_2Si composite. Thanks Qing-tao Guo for provision of electromagnetic stirrer and numerical simulation. This article was to mourn the passing of Dong Pan's beloved wife, Yi-tong Wang.

Conflict of interest

The authors declare that they have no known competing financial interests or personal relationships that could have appeared to influence the work reported in this paper. There is no professional or other personal interest of any nature or kind in any product, service and/or company that could be construed as influencing the position presented in, or the review of this manuscript.

References

[1] Wen T, Li Z C, Wang J Y, et al. From crack-prone to crack-free: Eliminating cracks in additively manufacturing of high-strength Mg_2Si-modified Al-Mg-Si alloys. J. Mater. Sci. Technol., 2025, 204: 276–291.

[2] Li C, Wu Y Y, Li H, et al. Morphological evolution and growth mechanism of primary Mg_2Si phase in Al-Mg_2Si alloy. Acta Mater., 2011, 59(3): 1058–1067.

[3] Shafieizad A H, Zarei-Hanzaki A, Abedi H R, et al. The Mg_2Si phase evolution during thermomechanical processing of in-situ aluminum matrix macro-composite. Mater. Sci. Eng. A, 2015, 644: 310–317.

[4] Chong X Y, Jiang W Q, Zhao Y G, et al. High performance of T6-treated Al-15Mg_2Si-3Cu composite reinforced with spherical primary Mg_2Si after the co-modification of Bi+Sr. Adv. Eng. Mater., 2019, 21(4): 1801119.

[5] Dong B X, Li Q, Wang Z F, et al. Enhancing strength-ductility synergy and mechanisms of Al-based composites by size-tunable in-situ TiB_2 particles with specific spatial distribution. Compos. Part. B–Eng., 2021, 217: 108912.

[6] Li Q, Dong B X, Liu T S, et al. Insight into solidification microstructure control by trace TiCN-TiB_2 particles for yielding fine-tuned nanoprecipitates in a hypoeutectic Al-Si-Mg alloy. Mater. Sci. Eng. A, 2021, 827: 142093.

[7] Tian X, Zhang D C, Wang K, et al. Microstructure and mechanical properties of high-pressure-assisted solidification of in situ Al-Mg_2Si composites. Mater. Sci. Eng. A, 2018, 733: 9–15.

[8] Zhang J, Fan Z, Wang Y, et al. Microstructural refinement in Al-Mg_2Si in situ composites. J. Mater. Sci. Lett., 1999, 18: 783–784.

[9] Qin Q D, Zhao Y G, Liu C, et al. Strontium modification and formation of cubic primary Mg_2Si crystals in Mg_2Si/Al composite. J. Alloy. Comp., 2008, 454: 142–146.

[10] Ghorbani M R, Emamy M, Khorshidi R, et al. Effect of Mn addition on the microstructure and tensile properties of Al-15%Mg_2Si composite. Mater. Sci. Eng. A, 2012, 550: 191–198.

[11] Nasiri N, Emamy M, Malekan A, et al. Microstructure and tensile properties of cast Al-15%Mg_2Si composite: Effects of phosphorous addition and heat treatment. Mater. Sci. Eng. A, 2012, 556: 446–453.

[12] Tebib M, Samuel A M, Ajersch F, et al. Effect of P and Sr additions on the microstructure of hypereutectic Al-15Si-14Mg-4Cu alloy. Mater. Charact., 2014, 89: 112–123.

[13] Wang H Y, Liu F, Chen L, et al. The effect of Sb addition on microstructures and tensile properties of extruded Al-20Mg_2Si-4Cu alloy. Mater. Sci. Eng. A, 2016, 657: 331–338.

[14] Wang Y, Guo X F. Heterogeneous nucleation of Mg_2Si and $Mg_2(Si,Sn)$ on Mg_3Sb_2 nucleus in Mg containing Si alloys. Mater. Charact., 2019, 233: 336–342.

[15] Cho W G, Kang C G. Mechanical properties and their microstructure evaluation in the thixoforming process of semi-solid aluminum alloys. J. Mater. Process. Technol., 2000, 105(3): 269–277.

[16] Li Y D, Hao Y, Yan F Y, et al. Microstructure evolution of AZ91D magnesium alloy during semi-solid isothermal heat treatment. Chinese J. Nonferrous. Met., 2011, 11: 571–575. (In Chinese)

[17] Nourouzi S, Kolahdooz A, Botkan M. Behavior of A356 alloy in semi-solid state produced by mechanical stirring. Adv. Mater. Res., 2011, 402: 331–336.

[18] Guo Q T, Wang T M, Jia J X, et al. Numerical study of flows driven by screw magnetic field in cylindrical container. Int. J. Cast Met. Res., 2013, 26: 92–99.

[19] Pan D, Guo Q T, Zhang K L, et al. Multi-physical fields distribution in billet during helical electromagnetic stirring: A numerical simulation research. China Foundry, 2024, 21(1): 51–59.

[20] Guo Q T, Tang X F, Li Z L, et al. Research on the influence of single winding helical electromagnetic stirring on the center segregation of high carbon large square billet. Mater. Rep., 2022, 36: 21010147. (In Chinese)

[21] Wang S B, Li J C. Numerical simulation of flow field and temperature field in continuous casting round billet under electromagnetic stirring. Foundry Technol., 2016, 37: 710–713. (In Chinese)

[22] Yang Z G, Wang B, Zhang X F, et al. Effect of electromagnetic stirring on molten steel flow and solidification in bloom mold. J. Iron Steel Res. Int., 2014, 21: 1095–1103.

[23] Bocklund B, Bobbio L D, Otis R A, et al. Experimental validation of Scheil-Gulliver simulations for gradient path planning in additively manufactured functionally graded materials. Materialia, 2020, 11: 100689.

[24] Wang R Y, Lu W H, Hogan L M. Faceted growth of silicon crystals in Al-Si alloys. Metall. Mater. Trans. A, 1997, 28: 1233–1243.

[25] Loue W R, Suery M. Microstructural evolution during partial remelting of Al-Si7Mg alloys. Mater. Sci. Eng. A, 1995, 203: 1–13.

[26] Soltani N, Bahrami A, Pech-Canul M I. The effect of Ti on mechanical properties of extruded in-situ Al-15 pct Mg_2Si composite. Metall. Mater. Trans. A, 2013, 44: 4366–4373.

[27] Zhang H, Chen M W, Ramesh K T, et al. Tensile behavior and dynamic failure of aluminum 6092/B_4C composites. Mater. Sci. Eng. A, 2006, 433: 70–82.

[28] Mcelroy R J, Szkopiak Z C. Dislocation substructure strengthening and mechanical thermal treatment of metals. Int. Met. Rev., 1972, 17: 175–202.

[29] Yan C K, Zhou Y C. Mechanical properties of Ti_2SnC particulate reinforced Cu matrix composites. Acta Metall. Sin., 2003, 39(1): 99–103. (In Chinese)

[30] Mullins W W, Sekerka R F. Morphological stability of a particle growing by diffusion or heat flow. J. Appl. Phys., 1963, 34: 323–329.

[31] Campanella T, Charbon C, Rappaz M. Grain refinement induced by electromagnetic stirring: A dendrite fragmentation criterion. Metall. Mater. Trans. A, 2004, 35: 3201–3210.

[32] Kurz W, Giovanola B, Trivedi R. Modeling of microsegregation in solidification of binary alloys. Acta. Metall., 1986, 34: 823–830.

[33] Ma G R, Li X L, Xiao L, et al. Effect of holding temperature on microstructure of an AS91 alloy during semisolid isothermal heat treatment. J. Alloy. Comp., 2010, 496: 577–581.

[34] Jin Y L, Fang H Z, Chen R R, et al. Graded distribution and refinement of Mg_2Si in Al-Mg_2Si alloy prepared by traveling magnetic field. J. Mater. Res. Technol., 2023, 24: 2319–2331.

[35] Song J X, Guo W L, Xing Z G, et al. Review of the effect of different magnetic field on metal solidification. China. Surf. Eng., 2023, 36: 1–20. (In Chinese)

[36] Han S F, Tan N, Wei K X, et al. Electromagnetic separation of silicon from metallurgical-grade silicon refined slag during the remelting process. Sep. Purif. Technol., 2022, 280: 119815. (In Chinese)

[37] Luo L, Luo L S, Su Y Q, et al. Reducing porosity and optimizing performance for Al-Cu-based alloys with large solidification intervals by coupling travelling magnetic fields with sequential solidification. J. Mater. Sci. Technol., 2021, 79: 1–14.

[38] Ghandvar H, Idris M H, Ahmad N. Effect of hot extrusion on microstructural evolution and tensile properties of Al-15%Mg_2Si-xGd in-situ composites. J. Alloy. Comp., 2018, 751: 370–390.

[39] Bai G Z, Liu Z, Lin J X, et al. Effects of the addition of lanthanum and ultrasonic stirring on the microstructure and mechanical properties of the in situ Mg_2Si/Al composites. Mater. Des., 2016, 90: 424–432.

[40] Ji S X, Yan F, Fan Z Y. Development of a high strength Al-Mg_2Si-Mg-Zn based alloy for high pressure die casting. Mater. Sci. Eng. A, 2015, 626: 165–174.

[41] Nazarizade B, Shabestari S G, Najaf Y. The effect of Cu-8%P master alloy, SIMA process, thixoforming, and heat treatment on the microstructure and mechanical properties of Al-20%Mg_2Si composite. J. Mater. Res. Technol., 2024, 30: 9183–9195.

[42] Ren Y Y, Chen S Y, Liu T Y, et al. Effect of Ti on microstructure and properties of electromagnetic stirred Al-18wt.%Mg_2Si alloy. China Foundry, 2023, 20(1): 78–82.

[43] Haghayeghi R, Zoqui E J, Halvaee A. An investigation on semi-solid Al-7Si-0.3Mg alloy produced by mechanical stirring. J. Mater. Process. Technol., 2005, 169: 382–387.

[44] Liu X B, Yang M, Zhao Y G, et al. Effect of isothermal time on microstructure and mechanical properties of semi-solid extruded Mg_2Si/Al composites. Heat Treat. Met., 2019, 44: 158–165. (In Chinese)

[45] Chegini M, Shaeri M H, Taghiabadi R, et al. Effect of equal channel angular pressing on microstructure and mechanical properties of thermally-homogenized Al-Mg_2Si composites. Mater. Chem. Phys., 2021, 259: 124200.

[46] Ren Y Y, Li Y M. Effect of phosphorus on microstructure and properties of Al-Mg_2Si alloys subjected to electromagnetic stirring. Adv. Mater. Res., 2011, 291–294: 652–657.

[47] Emamy M, Emami A R, Khorshidi R, et al. The effect of Fe-rich intermetallics on the microstructure, hardness and tensile properties of Al-Mg_2Si die-cast composite. Mater. Des., 2013, 46: 881–888.

[48] Malekan A, Emamy M, Rassizadehghani J, et al. The effect of solution temperature on the microstructure and tensile properties of Al-15%Mg_2Si composite. Mater. Des., 2011, 32: 2701–2709.

[49] Jiang W Q, Xu X F, Zhao Y G, et al. Effect of the addition of Sr modifier in different conditions on microstructure and mechanical properties of T6 treated Al-Mg_2Si in-situ composite. Mater. Sci. Eng. A, 2018, 721: 263–273.

[50] Yadav D K, Mahali M, Gupta S K, et al. Microstructural characterization and mechanical behavior of Al-4wt% Mg_2Si in-situ metal matrix composite synthesis via cooling slope casting technique. Mater. Today: Proc., 2022, 62: 442–447.